TOPOLOGICAL MATTER

Observation of topological superconductivity on the surface of an iron-based superconductor

Peng Zhang,[1]* Koichiro Yaji,[1] Takahiro Hashimoto,[1] Yuichi Ota,[1] Takeshi Kondo,[1] Kozo Okazaki,[1] Zhijun Wang,[2] Jinsheng Wen,[3] G. D. Gu,[4] Hong Ding,[5,6]* Shik Shin[1]*

Topological superconductors are predicted to host exotic Majorana states that obey non-Abelian statistics and can be used to implement a topological quantum computer. Most of the proposed topological superconductors are realized in difficult-to-fabricate heterostructures at very low temperatures. By using high-resolution spin-resolved and angle-resolved photoelectron spectroscopy, we find that the iron-based superconductor FeTe$_{1-x}$Se$_x$ (x = 0.45; superconducting transition temperature T_c = 14.5 kelvin) hosts Dirac-cone–type spin-helical surface states at the Fermi level; the surface states exhibit an s-wave superconducting gap below T_c. Our study shows that the surface states of FeTe$_{0.55}$Se$_{0.45}$ are topologically superconducting, providing a simple and possibly high-temperature platform for realizing Majorana states.

In a topological superconductor, the opening of the superconducting gap is associated with the emergence of zero-energy excitations that are their own antiparticles (1, 2). These zero-energy states, generally called Majorana zero modes or Majorana bound states (MBSs), have potential applications in quantum computing. One route to topological superconductivity is to realize a p-wave superconductor, which is an intrinsic topological superconductor; prominent candidates are Sr$_2$RuO$_4$ and Cu$_x$Bi$_2$Se$_3$. However, p-wave superconductivity is very sensitive to disorder, the experimental confirmation of the topological edge states is still elusive, and any application is highly challenging (3–5). Another way is to realize s-wave superconductivity on spin-helical states (6), such as in a topological insulator or a semiconductor with Rashba spin-split states

in proximity to a Bardeen-Cooper-Schrieffer (BCS) superconductor; some of the designs in this category have yielded strong experimental evidence of MBSs (7–11). However, this approach generally requires a long superconducting coherence length, which in principle prohibits the use of high-temperature superconductors. Additionally, the complicated heterostructures make further exploration and applications challenging. In this work, we show that the Fe-based superconductor FeTe$_{0.55}$Se$_{0.45}$, which can have a relatively high superconducting transition temperature T_c under certain conditions, hosts topological superconducting states on its surface, in accordance with theoretical predictions (12–14). This intrinsic topological superconductor, which takes advantage of the natural surface and interband superconducting coherence in the momentum space, can overcome the disadvantages of other implementations, paving a distinct route for realizing topological superconductivity and MBSs at higher temperatures.

First-principles calculations

Fe(Te,Se) has the simplest crystal structure among Fe-based superconductors (Fig. 1A), making it easy to obtain high-quality single crystals and thin films. Its T_c can reach ~30 K under pressure (15) and exceeds 40 K in monolayer thin films (16). Its in-plane electronic structure is similar to that of most of the iron-based superconductors: There are two hole-like Fermi surfaces (FSs) at the Brillouin zone (BZ) center (Γ) and two electron-like FSs at the BZ corner (M) (Fig. 1B). For a cut along ΓM, there are three hole-like bands (two of

Fig. 1. Band structure and topological superconductivity of FeTe$_{0.5}$Se$_{0.5}$.
(**A**) Crystal structure of Fe(Te,Se), together with the three-dimensional Brillouin zone (BZ) and projected-surface BZ. (**B**) Sketch of the in-plane BZ at $k_z = 0$ (**k** is the wave vector in reciprocal space). There are two hole-like FSs at Γ and two electron-like FSs at M. The dashed circle at Γ indicates a hole-like band just below E_F. (**C**) First-principles calculations of band structure along the ΓM direction (20),

indicated by the light blue line in (B). In the calculations, the energy scale t = 100 meV, whereas experiments yield t ~ 12 to 25 meV, depending on the bands (20). In this study, we focused on the small area around Γ shaded in light blue, where mainly the d$_{xz}$ band is present. (**D**) First-principles calculations of band structure along ΓM and ΓZ. The dashed box shows the SOC gap of the inverted bands. (**E**) Band structure projected onto the (001) surface. The topological surface states (TSSs) between the bulk valence band (BVB) and bulk conduction band (BCB) are evident. H, high intensity;

L, low intensity. (**F**) Superconducting (SC) states in the bulk and on the surface. The blue and red arrows illustrate the spin directions. The bulk states are spin-degenerated (black curves), whereas the TSSs are spin-polarized (blue and red curves). Below T_c, the bulk states open s-wave superconducting gaps, which are topologically trivial because of their spin degeneracy. Induced by the bulk-to-surface proximity, the TSSs open an s-wave gap and are topologically superconducting (TSC) as a consequence of the spin polarization (6). (The side surface is shown for convenience.)
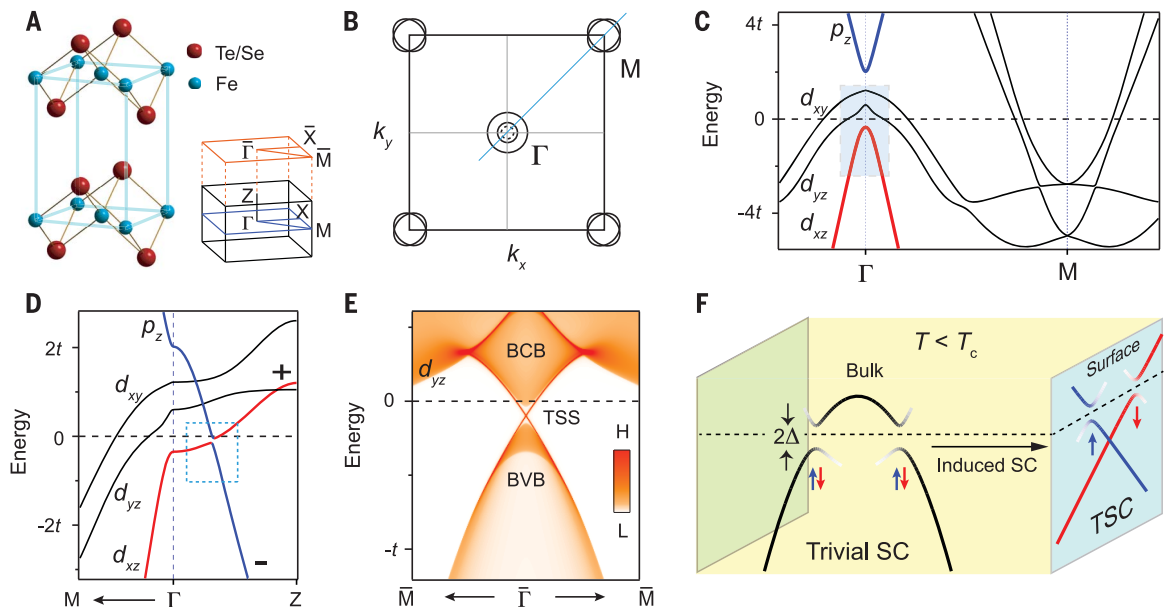
them crossing the Fermi level E_F) at Γ and two electron-like bands at M. Band calculations for the out-of-plane electronic structure predict that FeTe$_{0.5}$Se$_{0.5}$ has a nontrivial topology and hosts topological surface states near E_F (12–14).

Calculations show that the topological order originates from the Te substitution, which not only introduces large spin-orbit coupling (SOC) (17) but also shifts the p$_z$ band downward to E_F (12), whereas the p$_z$ band in FeSe or iron pnictides is generally above E_F (18, 19). Figure 1D shows the calculated band structure along ΓM and ΓZ (20). Along ΓZ, the p$_z$ band has a large dispersion; near E_F, SOC causes an avoided crossing with the d$_{xz}$ band, and a SOC gap opens. Further analysis shows that the p$_z$ band has an odd parity (–) for

^{1}Institute for Solid State Physics, University of Tokyo, Kashiwa, Chiba 277-8581, Japan. ^{2}Department of Physics, Princeton University, Princeton, NJ 08544, USA. ^{3}National Laboratory of Solid State Microstructures and Department of Physics, Nanjing University, Nanjing 210093, China. ^{4}Condensed Matter Physics and Materials Science Department, Brookhaven National Laboratory, Upton, NY 11973, USA. ^{5}Beijing National Laboratory for Condensed Matter Physics and Institute of Physics, Chinese Academy of Sciences, Beijing 100190, China. ^{6}CAS Center for Excellence in Topological Quantum Computation, University of Chinese Academy of Sciences, Beijing 100190, China.
*Corresponding author. Email: zhangpeng@issp.u-tokyo.ac.jp (P.Z.); dingh@iphy.ac.cn (H.D.); shin@issp.u-tokyo.ac.jp (S.S.)

the inversion symmetry, whereas the d$_{xz}$ band has an even parity (+). We note that the d$_{xz}$ band consists of mixed d$_{xz}$/d$_{yz}$ orbital characters along ΓZ. With these necessary ingredients, the calculated nontrivial topological invariance confirms that FeTe$_{0.5}$Se$_{0.5}$ hosts strong topological surface states near E_F (12). To show the predicted topological surface states clearly, we project the band structure onto the (001) surface in Fig. 1E. The Dirac-cone–type surface states are located near E_F, inside the SOC gap between the bulk valence band and the bulk conduction band. When FeTe$_{0.5}$Se$_{0.5}$ enters the superconducting state with s-wave gaps, superconductivity will be induced on the topological surface states, as shown in Fig. 1F. The spin polarization and s-wave superconductivity together would make the surface states topologically superconducting (6).

Dirac-cone–type spin-helical surface band and s-wave superconducting gap

To experimentally prove that FeTe$_x$Se$_{1–x}$ ($x \sim 0.5$) is a topological superconductor with intrinsic topological surface states and s-wave superconductivity on the surface, one needs to observe the following three phenomena in spectroscopic measurements: (i) Dirac-cone–type surface states; (ii) helical spin polarization of the surface states, which locks the spin direction perpendicular to the momentum

direction; and (iii) an s-wave superconducting gap of the surface states when $T < T_c$. Previously, we obtained some experimental evidence for the band inversion of the bulk p$_z$ and d$_{xz}$ bands (12, 21). However, the topological surface band was never directly observed, owing to the small energy and momentum scales. The SOC gap is estimated to be about 10 meV in the calculations, which makes it extremely difficult to resolve the Dirac-cone–type surface states in angle-resolved photoelectron spectroscopy (ARPES). In the previous ARPES experiments, only the three t$_{2g}$ (d$_{xy}$, d$_{yz}$, and d$_{xz}$) and the p$_z$ bulk bands were observed at Γ (12, 22, 23). In the experiment that we present below, by using ARPES with high energy and momentum resolution (HR-ARPES; energy resolution ~ 1.4 meV) (24) and spin-resolved ARPES (SARPES; energy resolution ~ 5.5 meV) (25), we were able to observe the three necessary phenomena required for the proof of topological superconductivity in high-quality single crystals of FeTe$_{0.55}$Se$_{0.45}$.

We first demonstrated the observation of the Dirac-cone–type surface states. High-resolution cuts of the band structure around Γ with p- and s-polarized photons are shown in Fig. 2, A and C, respectively. According to the matrix element effect [part I of (20)], both the surface and the bulk bands (p$_z$ and d$_{xz}$) should be visible for p-polarized photons, whereas only the bulk valence

Fig. 2. Dirac-cone–type surface band. (**A**) Band dispersion along ΓM, recorded with a p-polarized 7-eV laser. (**B**) MDC curvature plot of the data from (A), which enhances vertical bands (or the vertical part of one band) but suppresses horizontal bands (or the horizontal part of one band) (26). The red dots trace the points where the intensity of the MDC curvature exceeds the red bar in the color-scale indicator, and the blue lines are guides to the eye indicating the band dispersion. (**C**) Same as (A), but recorded with s-polarized light. The red line comes from the Lorentzian fitting of the EDC peaks. The red line is reproduced in (B) as a white line. (**D** and **E**) Zoomed-in view of the dashed box area in (A). The data are recorded at 2.4 K to reduce the thermal broadening. (D) EDCs of the zoomed-in area. The black and blue markers respectively trace the EDC peaks from two bands. arb., arbitrary. (E) EDC curvature plot of the zoomed-in area. The blue lines are the same as the ones in (B), and the red line is the same as the one in (C). (**F**) Summary of the overall band structure. The background image is a mix of raw intensity and EDC curvature (the area in the dashed box). The bottom hole-like band is the bulk valence band, whereas the Dirac-cone–type band is the surface band.
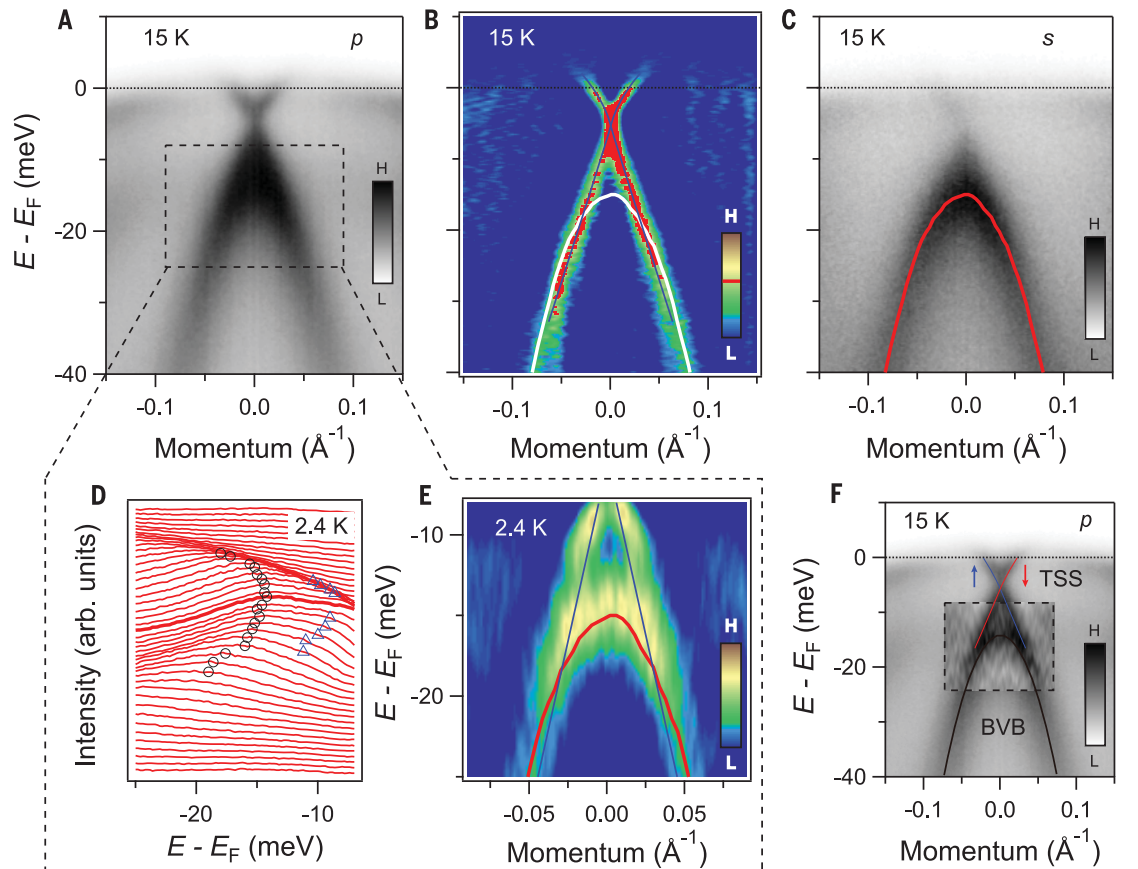
**Fig. 3. Spin-helical texture of the surface band.** (**A**) Sketch of the spin-helical FS and the band structure along k_y, the sample ΓM direction. The EDCs at cuts 1 and 2 were measured with SARPES. The spin pattern shown in (12) comes from the bottom surface. (**B**) Spin-resolved EDCs at cut 1. (**C**) Spin polarization curve at cut 1. (**D** and **E**) Same as (B) and (C), but for EDCs at cut 2. The measured spin polarizations are consistent with the spin-helical texture illustrated in (A). (**F**) Comparison of the EDCs from SARPES and HR-ARPES measurements. The large broadening in the SARPES measurement could be partly responsible for the small spin polarization measured in (C) and (E). a. u., arbitrary units.
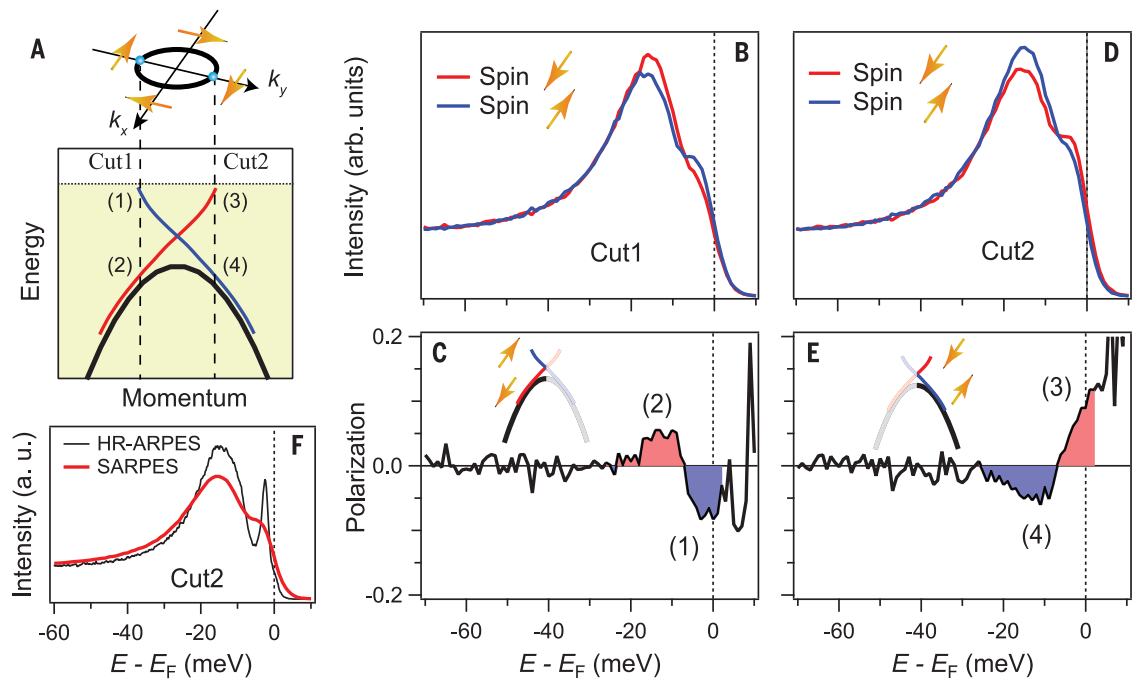
Fig. 4. s-wave superconducting gap of the surface band. (**A**) Raw EDCs at different temperatures for a position on the surface FS. The shoulders above E_F are the indication of the superconducting Bogoliubov quasiparticles. (**B**) Symmetrized EDCs of the curves shown in (A). (**C**) Superconducting gap size as a function of temperature. Data points are extracted from the coherence peaks in (B); error bars come from the uncertainty of the extraction. The inset shows the raw EDC at 7 K (black) and the EDC divided by the Fermi function (purple), which shows the Bogoliubov quasiparticles above E_F. (**D**) Symmetrized EDCs at different Fermi wave vectors (k_F) recorded at 2.4 K. The k_F positions of the cuts are indicated in (E). (**E**) Polar representation of the superconducting gap size. The hollow markers mirror the solid markers. The panel on the right shows the positions of measurements on the surface FS.
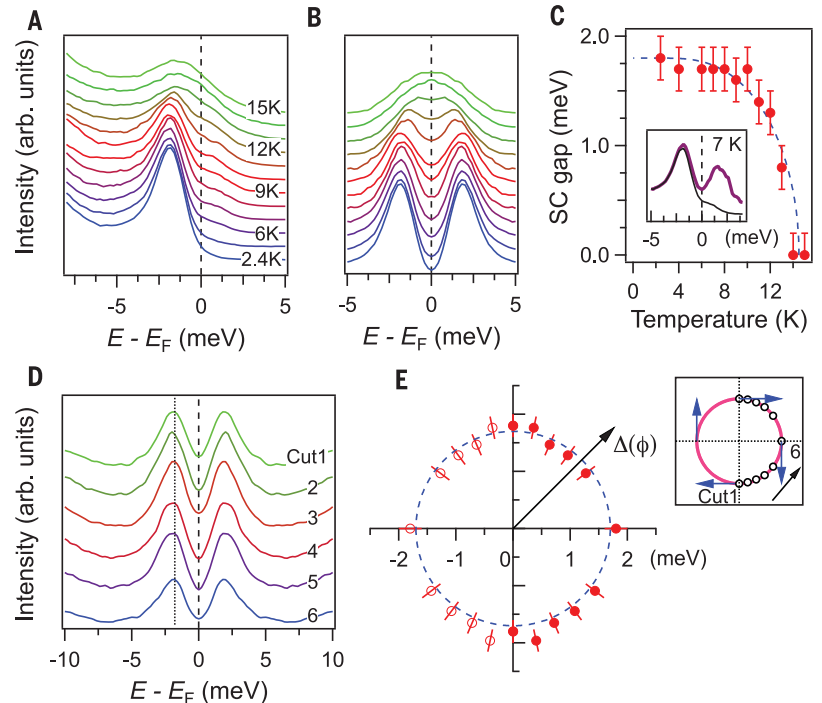

band (d_{xz}) is visible for s-polarized photons. The momentum distribution curve (MDC) curvature plot (an improved version of the second derivative method) (26) of the data with p-polarized photons shows a clear Dirac-cone–type band (Fig. 2B). We obtained a parabola-like band by extracting the energy distribution curve (EDC) peaks of the data with s-polarized photons (Fig. 2C). Combining the bands observed

in Fig. 2, A to C, we conclude that the Dirac-cone–type band (blue lines in Fig. 2B) is the topological surface band, and the parabolic band (white curve in Fig. 2B or red curve in Fig. 2C) is the bulk valence band. Further, we directly separated the bulk valence band from the Dirac-cone–type surface band with the data at very low temperature (2.4 K) when the spectral features were narrower (Fig. 2, D and E). We overlapped

the Dirac-cone–type surface band in Fig. 2B and the parabolic bulk band in Fig. 2C onto the EDC curvature plot in Fig. 2E. The extracted bands overlap well with the curvature intensity plot, confirming the existence of the parabolic bulk band and the Dirac-cone–type surface band. The overall band structure is summarized in Fig. 2F, demonstrating a Dirac surface band very close to E_F.

Fig. 5. Topological superconductivity and Majorana states on the surface. (**A**) Topological superconductivity on the surface of $FeTe_{0.55}Se_{0.45}$. The electrons in the bulk are not spin-polarized, and the s-wave superconducting pairing is topologically trivial. The electrons on the surface are induced to form superconducting pairs by the bulk superconductivity. The superconductivity of the spin-helical surface states is topologically nontrivial. (**B**) A magnetic field creates vortices in $FeTe_{0.55}Se_{0.45}$, which behave as boundaries for the topological superconductivity on the surface. MBSs are expected to appear in the vortices. If there is a magnetic domain on the surface that destroys superconductivity within that domain, there will be itinerant Majorana modes along the boundary of the domain.
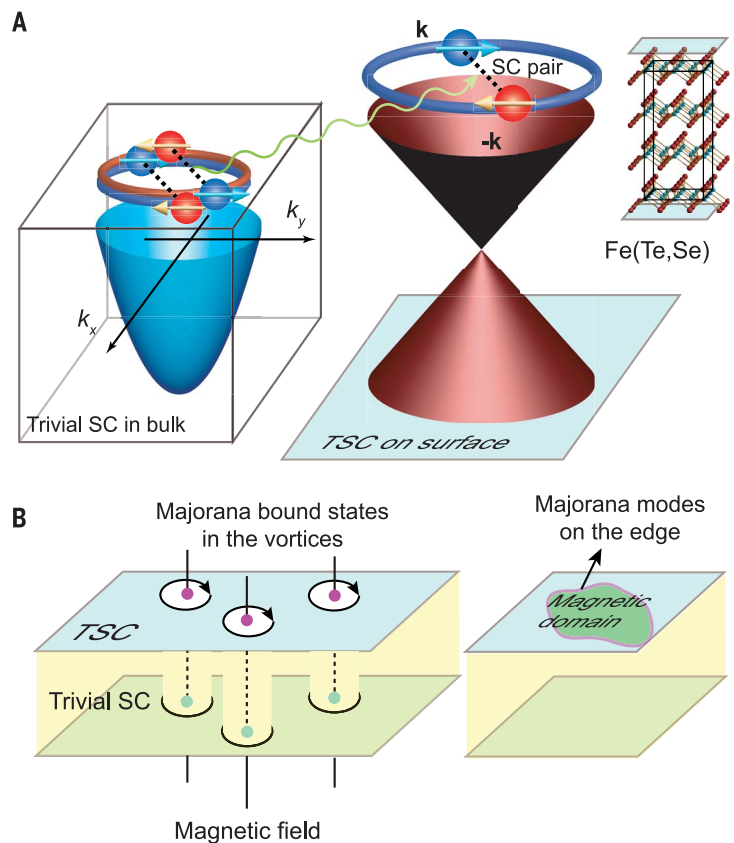
Next, we carried out high-resolution spin-resolved experiments to check the spin polarization of the Dirac-cone–type band. Two EDCs at the cuts indicated in Fig. 3A were measured. If the Dirac-cone–type band comes from the spin-polarized surface states, the EDCs at cuts 1 and 2 should show reversed spin polarizations. Indeed, the spin-resolved EDCs in Fig. 3, B and D, show that the spin polarizations are reversed for cuts 1 and 2, whereas the background shows no spin polarization (Fig. 3, C and E). These data are consistent with the spin-helical texture, which is the direct consequence of "spin-momentum locking" of topological surface states. We also measured an additional two EDCs at different positions on the FS [part III of (20)]. The spin polarizations of all four EDCs are consistent with the spin-helical texture predicted by theory (12). The small magnitude of the spin polarizations in Fig. 3, C and E, may partly be explained by the large broadening of the SARPES data, originating from the lower resolution of that technique (Fig. 3F).

As the final piece of evidence, we show the opening of an s-wave gap for the topological surface band. Figure 4A displays the evolution of one EDC from the surface band with temperature. The superconducting coherence peak gradually builds up with decreasing temperature; the symmetrized EDCs in Fig. 4B show the gap closing above T_c. The relation between the superconducting gap size and temperature (Fig. 4C) agrees well with BCS theory. The EDC divided by the corresponding Fermi function (Fig. 4C, inset) shows a clear peak at the symmetric position

above E_F, which comes from the particle-hole mixing of the Bogoliubov quasiparticles, thus proving the superconducting nature of the coherence peak. The momentum-dependent measurement of the superconducting gap size shows no anisotropy (Fig. 4, D and E), consistent with the s-wave superconducting nature of iron-based superconductors (27–29). The gap size of the surface band is about 1.8 meV, which is smaller than the bulk gap size of 2.5 meV for the hole band and 4.2 meV for the electron band, as reported in (27, 28). This result is consistent with induced superconductivity on the surface and may even suggest that the induced superconductivity mainly comes from interband scattering from the neighboring hole-like band.

Prospects for the observation of Majorana states

We summarize our results in Fig. 5A. A Dirac-cone–type topological surface band exists on the surface of $FeTe_{0.55}Se_{0.45}$. When the bulk bands open superconducting gaps, s-wave superconductivity is induced in the surface band through interband scattering. Because of its spin-helical texture, the surface band exhibits topological superconductivity, whereas the bulk superconductivity is topologically trivial. When an external magnetic field is applied, a pair of MBSs is expected to appear at the two ends of the vortices (Fig. 5B). This physical picture may explain the recent observations of zero-bias peaks in this material (30, 31). Furthermore, if a magnetic domain is deposited on the surface, destroying superconductivity within that

domain, there should be itinerant Majorana modes along the domain edge. As a result of the intrinsic topological superconductivity on the natural surface, it should be fairly easy to produce MBSs and Majorana edge modes. The relatively high T_c and facile growth of high-quality single crystals and thin films make Fe(Te,Se) a promising platform for studying MBSs and may further advance research on quantum computing.

REFERENCES AND NOTES

1. X.-L. Qi, S.-C. Zhang, *Rev. Mod. Phys.* **83**, 1057–1110 (2011).
2. C. Nayak, S. H. Simon, A. Stern, M. Freedman, S. Das Sarma, *Rev. Mod. Phys.* **80**, 1083–1159 (2008).
3. L. Fu, E. Berg, *Phys. Rev. Lett.* **105**, 097001 (2010).
4. S. Sasaki *et al.*, *Phys. Rev. Lett.* **107**, 217001 (2011).
5. N. Levy *et al.*, *Phys. Rev. Lett.* **110**, 117001 (2013).
6. L. Fu, C. L. Kane, *Phys. Rev. Lett.* **100**, 096407 (2008).
7. V. Mourik *et al.*, *Science* **336**, 1003–1007 (2012).
8. S. Nadj-Perge *et al.*, *Science* **346**, 602–607 (2014).
9. S. M. Albrecht *et al.*, *Nature* **531**, 206–209 (2016).
10. S.-Y. Xu *et al.*, *Nat. Phys.* **10**, 943–950 (2014).
11. H.-H. Sun *et al.*, *Phys. Rev. Lett.* **116**, 257003 (2016).
12. Z. Wang *et al.*, *Phys. Rev. B* **92**, 115119 (2015).
13. X. Wu, S. Qin, Y. Liang, H. Fan, J. Hu, *Phys. Rev. B* **93**, 115129 (2016).
14. G. Xu, B. Lian, P. Tang, X.-L. Qi, S.-C. Zhang, *Phys. Rev. Lett.* **117**, 047001 (2016).
15. K. Horigane, N. Takeshita, C.-H. Lee, H. Hiraka, K. Yamada, *J. Phys. Soc. Jpn.* **78**, 063705 (2009).
16. F. Li *et al.*, *Phys. Rev. B* **91**, 220503 (2015).
17. P. D. Johnson *et al.*, *Phys. Rev. Lett.* **114**, 167001 (2015).
18. S. Graser *et al.*, *Phys. Rev. B* **81**, 214503 (2010).
19. H. Eschrig, A. Lankau, K. Koepernik, *Phys. Rev. B* **81**, 155447 (2010).
20. Supplementary materials.
21. X. Shi *et al.*, *Sci. Bull.* **62**, 503–507 (2017).
22. Y. Lubashevsky, E. Lahoud, K. Chashka, D. Podolsky, A. Kanigel, *Nat. Phys.* **8**, 309–312 (2012).

23. P. Zhang et al., Appl. Phys. Lett. **105**, 172601 (2014).
24. K. Okazaki et al., Science **337**, 1314–1317 (2012).
25. K. Yaji et al., Rev. Sci. Instrum. **87**, 053111 (2016).
26. P. Zhang et al., Rev. Sci. Instrum. **82**, 043712 (2011).
27. H. Miao et al., Phys. Rev. B **85**, 094506 (2012).
28. K. Okazaki et al., Sci. Rep. **4**, 4109 (2014).
29. D. C. Johnston, Adv. Phys. **59**, 803–1061 (2010).
30. F. Massee et al., Sci. Adv. **1**, e1500033 (2015).
31. J.-X. Yin et al., Nat. Phys. **11**, 543–546 (2015).

SUPPLEMENTARY MATERIALS

www.sciencemag.org/content/360/6385/182/suppl/DC1
Materials and Methods
Supplementary Text
Figs. S1 to S3
Table S1
References (32–41)
Data S1

16 April 2017; accepted 2 February 2018
Published online 8 March 2018
10.1126/science.aan4596

Science

Observation of topological superconductivity on the surface of an iron-based superconductor

Peng Zhang, Koichiro Yaji, Takahiro Hashimoto, Yuichi Ota, Takeshi Kondo, Kozo Okazaki, Zhijun Wang, Jinsheng Wen, G. D. Gu, Hong Ding and Shik Shin

A topological superconductor

A promising path toward topological quantum computing involves exotic quasiparticles called the Majorana bound states (MBSs). MBSs have been observed in heterostructures that require careful nanofabrication, but the complexity of such systems makes further progress tricky. Zhang *et al.* identified a topological superconductor in which MBSs may be observed in a simpler way by looking into the cores of vortices induced by an external magnetic field. Using angle-resolved photoemission, the researchers found that the surface of the iron superconductor $FeTe_{0.55}Se_{0.45}$ satisfies the required conditions for topological superconductivity.

Science, this issue p. 182

ARTICLE TOOLS	http://science.sciencemag.org/content/360/6385/182
SUPPLEMENTARY MATERIALS	http://science.sciencemag.org/content/suppl/2018/03/07/science.aan4596.DC1
REFERENCES	This article cites 40 articles, 4 of which you can access for free http://science.sciencemag.org/content/360/6385/182#BIBL
PERMISSIONS	http://www.sciencemag.org/help/reprints-and-permissions

Use of this article is subject to the Terms of Service